Journal of Structural Geology 33 (2011) 1611–1626

Contents lists available at SciVerse ScienceDirect

Journal of Structural Geology

journal homepage: www.elsevier.com/locate/jsg

Development of a self-similar strike-slip duplex system in the Atacama Fault system, Chile

E. Jensen[a,*], J. Cembrano[b], D. Faulkner[c], E. Veloso[a], G. Arancibia[b]

[a] Departamento de Ciencias Geológicas, Universidad Católica del Norte, Antofagasta, Avenida Angamos 0610, Antofagasta, Chile
[b] Departamento de Ingeniería Estructural y Geotécnica, Pontificia Universidad Católica de Chile, Santiago, Vicuña Mackenna 4860, Macul, Santiago, Chile
[c] Rock Deformation Laboratory, Department of Earth and Ocean Sciences, University of Liverpool, Liverpool L69 3BX, United Kingdom

ARTICLE INFO

Article history:
Received 2 December 2010
Received in revised form
10 August 2011
Accepted 1 September 2011
Available online 16 September 2011

Keywords:
Fault internal structure
Strike-slip duplex
Self-similarity
Fault development
Fracture network

ABSTRACT

Fault development models are crucial to predict geometry and distribution of fractures at all scales. We present here structures related to the development of the Bolfín Fault in the Atacama Fault System (AFS), covering a range of scales of 7 orders of magnitude. The AFS is a 1000 km-long trench-parallel fault system located in the Andean Forearc. The Bolfín Fault is a first-order fault of the Caleta Coloso Duplex, has a trend ~170° and length >45 km. It cuts mainly meta-diorites and exhibits a 100–200 m thick core of subvertical bands of altered fractured host rock and of foliated cataclasites. This foliation is made up of several trend-parallel cm-thick shear bands, composed of plagioclase fragments (>0.1 mm) surrounded by epidote.

In the compressive quadrant around the tip point of Bolfín Fault, the lower strain faults exhibit an unusual internal structure consisting of fractures arranged in a multi-duplex pattern. This pattern can be observed from meters to millimeters scale. The fractures in the strike-slip duplex pattern can be separated into two types. *Main Faults*: trend-parallel, longer and with larger offsets; and *Secondary Fractures*: sigmoid-shape fractures distributed in the regions between Main Faults, all oriented between 15° and 75° with respect to the Main Faults, measured counterclockwise (i.e. in P-diedra).

On the basis of the distribution of the two types of recognized fractures, the relative sequence of propagation can be inferred. Main Faults, the more widely distributed, propagated earlier. The Secondary Fractures, in turn, distributed in thinner areas between the larger Main Faults, were propagated later as linking fractures.

The duplex pattern is self-similar: Multiple-Core Faults with internal structure of multiple-duplex are itself in turn secondary faults within a larger km-scale duplex (Caleta Coloso Duplex).

The duplex width (W) and the length (L) of the Main Faults forming the duplex show an almost linear relationship, for duplexes observed from micro- to regional scale. For a scale range of seven orders of magnitude, the length of the master strike-slip faults is about ten times the width of the overlapping duplex area. This relationship evidence the self-similar nature of the structural system under study and suggests that the same fundamental mechanical processes that build up the small strike-slip duplexes operate also at the regional scale.

1. Introduction

The progressive development of the geometric arrangement of faults in the upper crust is of fundamental importance for a host of applications such as ore deposit exploration, hydrocarbon reservoir production and for the understanding of intra-plate seismicity. Faults localize ore bodies through their fundamental control of fluid flow (Sibson et al., 1975; Barton et al., 1995; Connolly and Cosgrove, 1999; Cox, 1999; Sanderson and Zhang, 2004; Sibson, 1987, 1994; Wibberley et al., 2008) and the displacement of pre-existing ore bodies (Sillitoe, 1973; Tomlinson and Blanco, 1997a,b). In hydrocarbon fields, faults transport and trap oil and gas (Gibson, 1994; Smith, 1980). In seismology, in turn, the geometry of faults systems controls the distribution of the intra-plate seismicity by rupturing and fracturing (Lange et al., 2008; Sibson, 1985; Sylvester, 1988). Therefore, conceptual models about how faults propagate and develop in the upper crust are

* Corresponding author. Tel.: +56 55 355972; fax: +56 9 95789625.
E-mail addresses: erikjensen@ucn.cl (E. Jensen), jcembrano@ing.puc.cl (J. Cembrano), faulkner@liv.ac.uk (D. Faulkner), eveloso@ucn.cl (E. Veloso), garancibia@ing.puc.cl (G. Arancibia).

0191-8141/$ – see front matter © 2011 Elsevier Ltd. All rights reserved.
doi:10.1016/j.jsg.2011.09.002

crucial for studying those topics that demand knowledge of fault geometry.

Models of fault propagation and growth have been constructed from the observations and analysis of faulted laboratory samples (Lockner et al., 1991; Scholz et al., 1993; Wibberley et al., 2000) to the observation and measurement of mesoscopic- to regional-scale faults (Cembrano et al., 2005; Flodin and Aydin, 2004; Martel et al., 1988; Moir et al., in press; Swanson, 2006). Nonetheless, they are based on observations over a small-scale range whereas models including structures from micro- to regional-scale are very scarce (*e.g.* Martel et al., 1988), mainly because of the lack of fault zones exhibiting well-exposed fractures at all scales.

Here, we present and analyze structures related to the propagation and evolution of the Atacama Fault System (AFS) in the Coastal Cordillera of Northern Chile (Arabasz, 1971; Scheuber and Andriessen, 1990) exhumed from seismogenic depths (6–10 km) and observed over a range of scale of 7 orders of magnitude (10^{-4} to 10^{4} m). An excellent exposure of faults results from very slow erosion in the coastal-desert climate (Fuenzalida, 1965) and allows a rigorous analysis of structures from micro- to regional-scale. All of the faults analyzed here cut essentially the same protolith, and hence direct comparisons can be made over the range of scales. We are then able to present excellent milimetric-scale structures that provide data about the fault geometry evolution at small scale, and structural maps, showing the medium (meter-scale) and large (km-scale) scale fault arrangements. These multi-scale observations and measurements are analyzed, in terms of orientation, size and displacement, to construct a model of propagation and development of a strike-slip duplex fault system. The observations are compared with previously published work from other natural fault systems.

In this paper, the term *fracture* is used to refer any petrographic or crystallographic planar and relatively narrow discontinuity, disrupting the original physical properties of a rock. This term is used regardless of the relative movement of the volumes of solid separated by the fracture, and hence it includes ex*tensional fractures* (also *cracks* or *joints*) and *shear fractures* (or *faults,* defined below). If some other material is filling a fracture, the structure is named according to the nature of this material (*e.g.* dyke or vein).

The term *fault* is used specifically to refer to *shear fractures*, that is, a relatively narrow discontinuity with observable shear offset at a given scale. An oriented group of faults with a preferred orientation concentrated in a narrow planar zone is referred as a single fault if the scale of observation means that it can be represented only with a line.

2. Regional structural setting

2.1. The Atacama Fault System (AFS)

The Atacama Fault System or AFS (Fig. 1A) is the most important tectonic feature of the Coastal Cordillera in the Central Andes forearc (Arabasz, 1971; Brown et al., 1993; Grocott and Taylor, 2002; Scheuber and Andriessen, 1990). It is a trench-parallel fault system (Scheuber and González, 1999) composed of several subvertical and NS to NW-striking, fault segments ranging up to tens of kilometers in length. These segments are organized into a ~1000 km-long and ~50 km-thick fault system, affecting the Jurassic magmatic arc between Iquique (21°S) and La Serena (30°S) (Arabasz, 1971; Brown et al., 1993; González, 1996).

The deformation in the Coastal Cordillera has been interpreted to be strongly controlled by the magmatic activity of the Jurassic–Early Cretaceous arc, from 200 to 120 Ma ago (Scheuber and Reutter, 1992). The AFS *sensu stricto* propagated in the last stages of deformation, when the progressive cooling of the arc led to a change in the mode of deformation from a plastic regime represented by kilometric shear zones of amphibolite (150–143 Ma) to greenschist facies (139–125 Ma) (Scheuber et al., 1995) and finally to a brittle regime represented by meter-thick fault cores of chlorite- and epidote-rich cataclasites (125–118 Ma) that form the main structure of the AFS (Cembrano et al., 2005). Crosscutting relationships plus these common alteration products indicate that these brittle structures formed under the same physical conditions and during the same deformation episode. This paper focuses on the progressive development of small- to large-scale structures during the brittle propagation stage of a segment of the AFS.

The kinematics of the brittle structures of the AFS is mainly left-lateral strike-slip with a minor extensional component. This kinematics has been attributed to the highly oblique convergence in the subduction of the Aluk plate under the South American plate during the Mesozoic (Grocott and Taylor, 2002; Scheuber and Andriessen, 1990; Scheuber and González, 1999)

Cenozoic normal movements have also been recorded in the AFS, attributed to elastic rebound of the forearc co-seismically with large magnitude subduction earthquakes (Gonzalez and Carrizo, 2003). These are easy to recognize in the field as localized subvertical brittle structures that do not greatly overprint the earlier, more widespread brittle deformation. The structures temporally associated with these later movements will not be described as they are not on the focus of this paper.

2.2. The Caleta Coloso Duplex (CCD)

The CCD is a strike-slip structure located 20 km south from Antofagasta (Fig. 1A). It is formed by two, NNW-striking, subvertical master faults that splay off the Coloso Fault, a major structure of the AFS. These two master faults are the Bolfin and Jorgillo Faults (Fig. 1B), which are in turn joined by a set of second-order NW-striking and third-order EW-striking, imbricate splay faults. The CCD has been interpreted to be formed in a dilatational jog between Jorgillo and Bolfin Faults (Cembrano et al., 2005; González, 1996).

According to previous work, the second-order faults in the CCD have southwestward steep dips and left-lateral/normal kinematics; they have minimum net displacements varying between 10 and 100 m and show variable internal structure. Low-displacement faults (in the order of 1–10 m) consist of straight decameter-long faults linked by hybrid/extensional fractures, and high displacement faults (of the order of >10 m) show well-developed layers of cataclasites and gouge (Cembrano et al., 2005).

The third-order faults, in turn, are steeply to shallowly dipping both to the south and north with mainly normal kinematics; they have centimetric thickness and vertical separations between 1 and 10 cm (Herrera et al., 2005; Olivares, 2004).

The physical conditions under which the CCD was developed can be inferred from the associated mineral assemblages. Both the cataclasites from the fault cores and spatially and geometrically related hydrothermal veins show mineral assemblages of epidote, chlorite and quartz, suggesting a strong link between faulting and fluid transport under low-greenschist facies conditions (Cembrano et al., 2005; Olivares, 2004). The depths from which the rocks have been passively exhumed have been estimated between 3 km and 10 km (Faulkner et al., 2006; Herrera et al., 2005).

3. Methodology

For characterizing the geometry of regional-scale faults (1–10 km-long), our observations are based on detailed maps (1:250,000 to 1:100,000 scale) and descriptions made by several

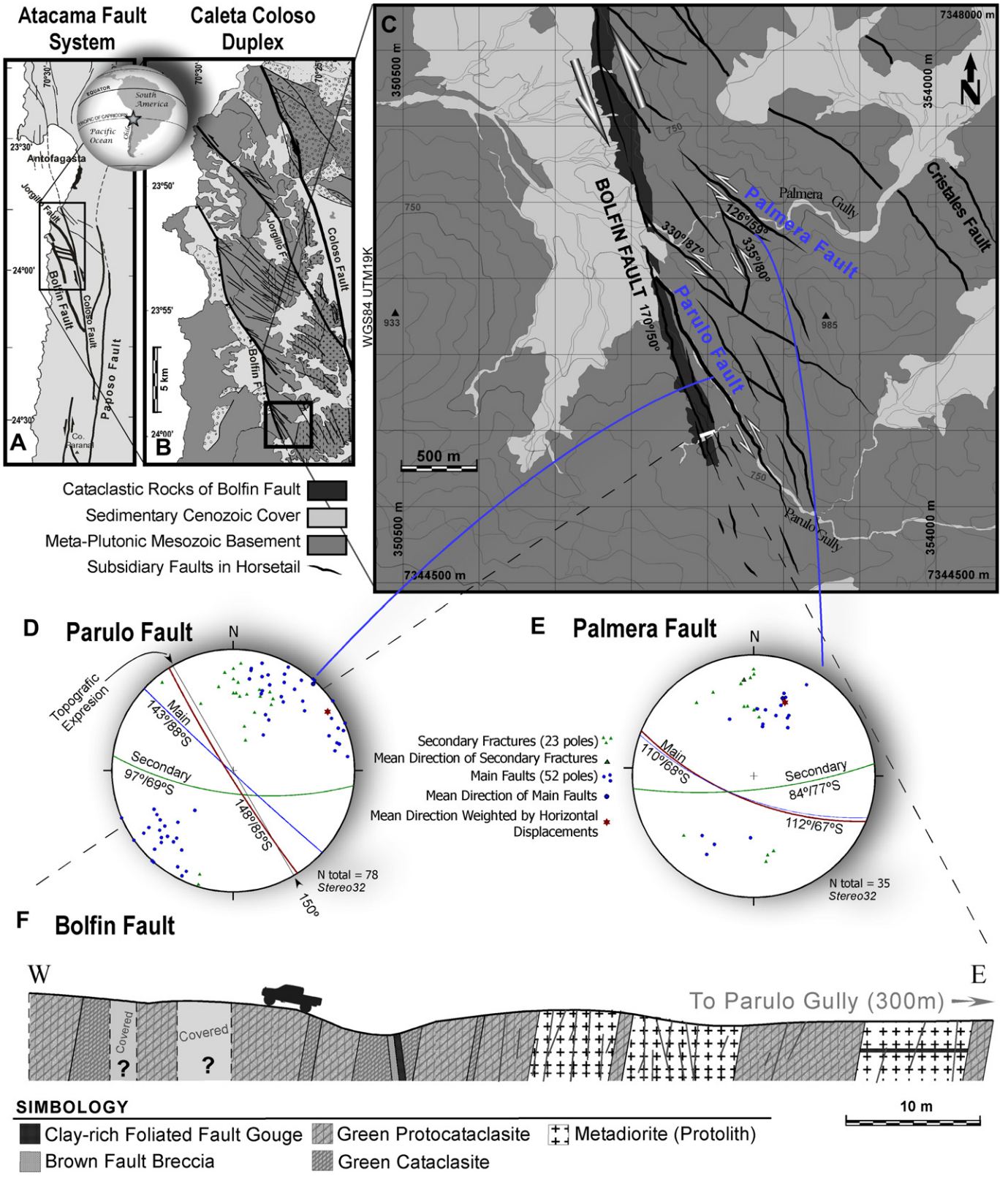

Fig. 1. Kilometric-scale structural maps: (A) regional scale map showing the geometry of Atacama Fault System in Antofagasta Region, Chile (simplified from Brown et al., 1993). (B) Map of the Duplex Caleta Coloso, redrawn from Cembrano et al. (2005). (C) Map of the horsetail structure in a termination (tip point) of Bolfin Fault. Parulo and Palmera Faults are described in the text. (D) and (E) Equal-area projection diagrams of fractures measured within the Parulo and Palmera Faults, respectively (data in Tables 1 and 2). Triangles and dots are the poles of Secondary Fractures and Main Faults respectively, and the lines represent the great circles of the calculated mean directions (blue: Main Faults, green: Secondary Fractures). Weighted mean orientation is plotted in dark red and was calculated weighting the fracture orientations by the horizontal displacement of them. (F) Vertical section perpendicular to the strike of the Bolfin Fault close to the tip. (For interpretation of the references to colour in this figure legend, the reader is referred to the web version of this article.)

previous studies in the AFS and Caleta Coloso Duplex (Arabasz, 1971; Cembrano et al., 2005; González, 1996; Olivares, 2004). For meter- to hundred-meters scale faults (10^1 to 10^2 m long), mapping at 1:10,000 scale was carried out at the tip point of one segment of a regional-scale fault, the Bolfin Fault. The tip point was selected because of good exposure and the occurrence of several spatially related faults, which at larger scale appear to form a horsetail structure (Fig. 1B) (Cembrano et al., 2005; Herrera et al., 2005; Olivares, 2004). The tip point is thought to represent a zone of possible static and dynamic fracturing resulting from fault propagation and/or arrest (Faulkner et al., 2011).

The outcrop-scale fractures (10^{-3} to 10^1 m long), which constitute the internal structure of larger scale faults, were characterized and measured by means of detailed outcrop-scale maps, made at the 1:20 and 1:5 scales. These maps were produced directly in the field, based on structural measurements and on digital camera imaging. For the case of the internal structure of the Parulo Fault (Fig. 2), the map (10^{-1} to 10^1 m) was constructed onto an ortho-rectified photomosaic, composed of 196 images with a spatial resolution of 10 mm. These images were obtained with a 5.36 Mp camera mounted on a structure consisting of 4 fixed legs connected by 4 metallic cables, forming a 7 m horizontal square. The images where rectified and stitched together with the Orthobase application of Erdas Imagine, taking into account the distance of the camera, the position, focal distance, and some reference points previously marked in the outcrop before the imaging (Fig. 3).

The microscopic-scale deformation (10^{-5} to 10^{-3} m long fractures) was characterized by fracture counting and mapping on oriented thin sections, taken both from the core of the main regional-scale fault (Bolfin Fault) of the studied area and from the damage zones of the surrounding outcrop-scale faults (Palmera Fault).

In the Palmera Fault, the microanalysis was conducted directly on the M plane (a plane orthogonal to the fault and parallel to the striae). This configuration allows measuring the real angles between the main shear plane (the faulting plane in this case) and the

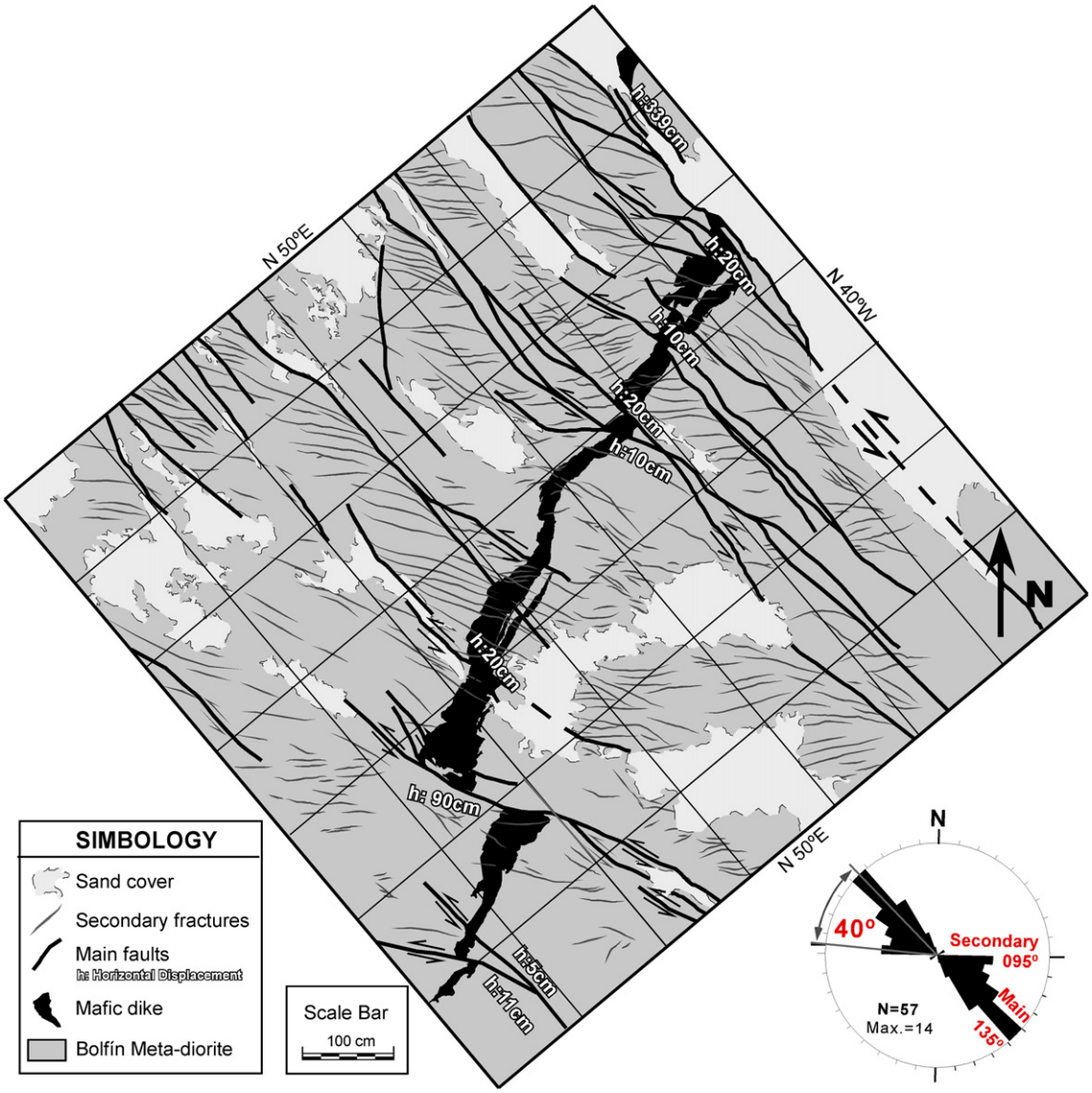

Fig. 2. Outcrop-scale structural map in Parulo Fault. Performed over the ortho-rectified photomosaic of Fig. 3. The black band is a displaced mafic dike. White numbers are horizontal offsets (h). The protolith, or host rock, is metadiorite of the Bolfin Complex. The rose diagram in the lower right shows that the Secondary Fractures have an average trend 40° counterclockwise from Main Faults. (For interpretation of the references to colour in this figure legend, the reader is referred to the web version of this article.)

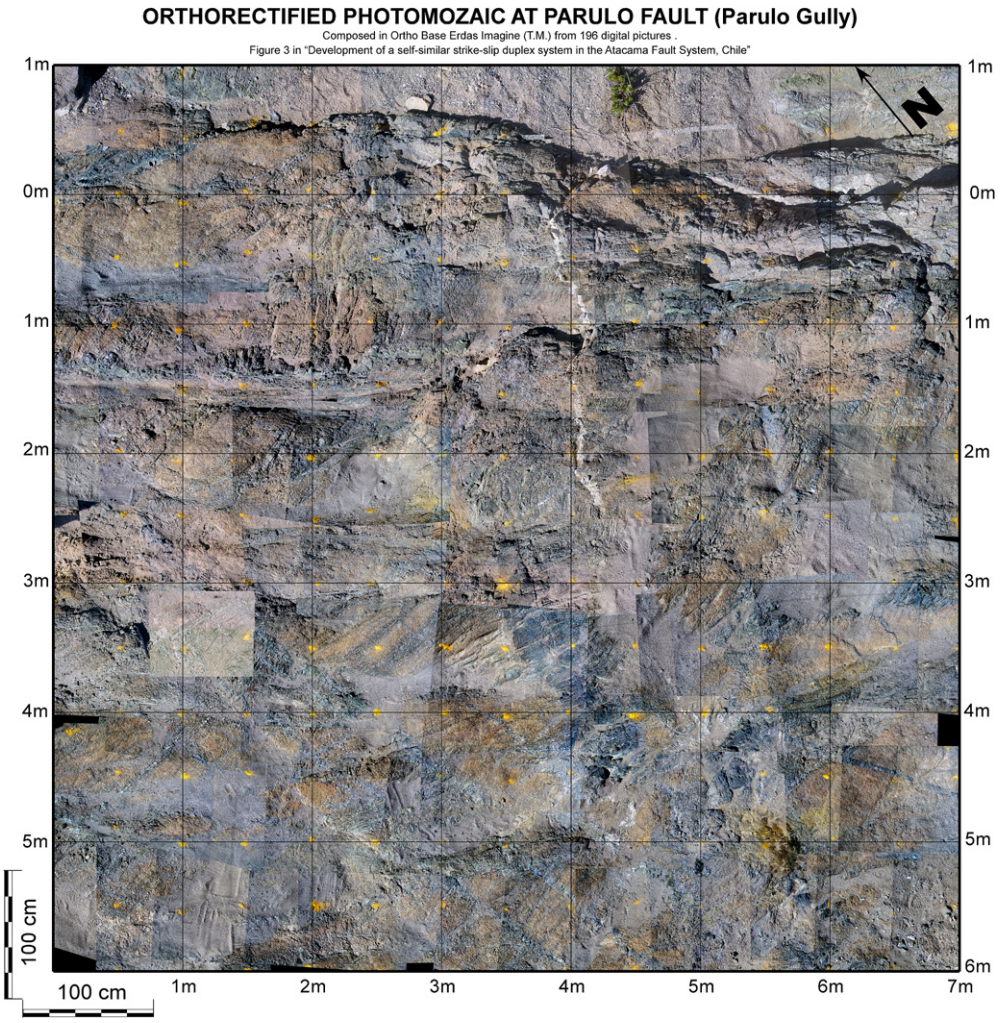

Fig. 3. Ortho-rectified photomosaic of a sub-horizontal outcrop in the internal structure of Parulo Fault. Base of mapping to build the map on Fig. 2.

spatially related fractures. Then, the real orientation of the related fractures can easily be traced on a stereographic projection as a lineation contained in the known M-plane.

4. Fault system description

The Bolfin Fault splays off the Coloso Fault at 70°23′ 24°10′, with an average strike of 162° and an exposed length of at least 45 km. It has a 50–100 m-thick core, with an internal structure characterized by subvertical meter-thick zones of cohesive fault rocks and of some fractured host rock, very similar to that described for the Coloso Fault (Cembrano et al., 2005; Faulkner et al., 2006, 2008). Fault rocks are mainly dark green cataclasite and protocataclasite (according to classification by Sibson, 1977) with 2 discrete strands, 2–50 to 80 cm thick of brown/red foliated gouge. The dark green color of the cohesive rocks is given by the epidote–chlorite mineral association, mainly cementing rock fragments and in veins, but also altering original minerals in the host rock. The red color of the gouge is due to oxidized iron-bearing minerals such as hematite.

The Bolfin Fault is segmented into three main sections; the southern termination of the central fault segment is the focus of this study, as it shows the best developed small-to-large-scale fault zone structure (Fig. 1B).

In this region, the Bolfin Fault exhibits several related smaller faults arranged in a horsetail structure consistently orientated with the kilometric geometry of the Caleta Coloso Duplex (Cembrano et al., 2005; Herrera et al., 2005; Olivares, 2004).

All faults mapped in this termination area are located to the East of Bolfin Fault, are NW-striking, have subvertical dips (between 70°SW and 70°NE) and trace lengths between 300 m and 3 km (Fig. 1C).

Two types of faults can be identified according their internal structure at the outcrop-scale: *Single-Core Faults* and *Multiple Strand Faults.*

4.1. Single-core faults

The traces of these faults are easy to recognize in the high-resolution satellite images and can be seen as continuous straight lines. These are the most frequently mapped faults in previous works and a good example of one of these faults is the Cristales Fault (Fig. 1C and see also Mitchell and Faulkner, 2009).

The single-core faults show a single green cataclastic core similar to that of Bolfin Fault but thinner, generally 0.5–2 m total thick, and with less bands. The cores exhibits two sets of different planar structures (foliations), one defined by compositional and textural bands, and another defined by discrete preferentially oriented discontinuities (fractures).The former are sub-parallel to the core boundaries and consist of layers of different colors and

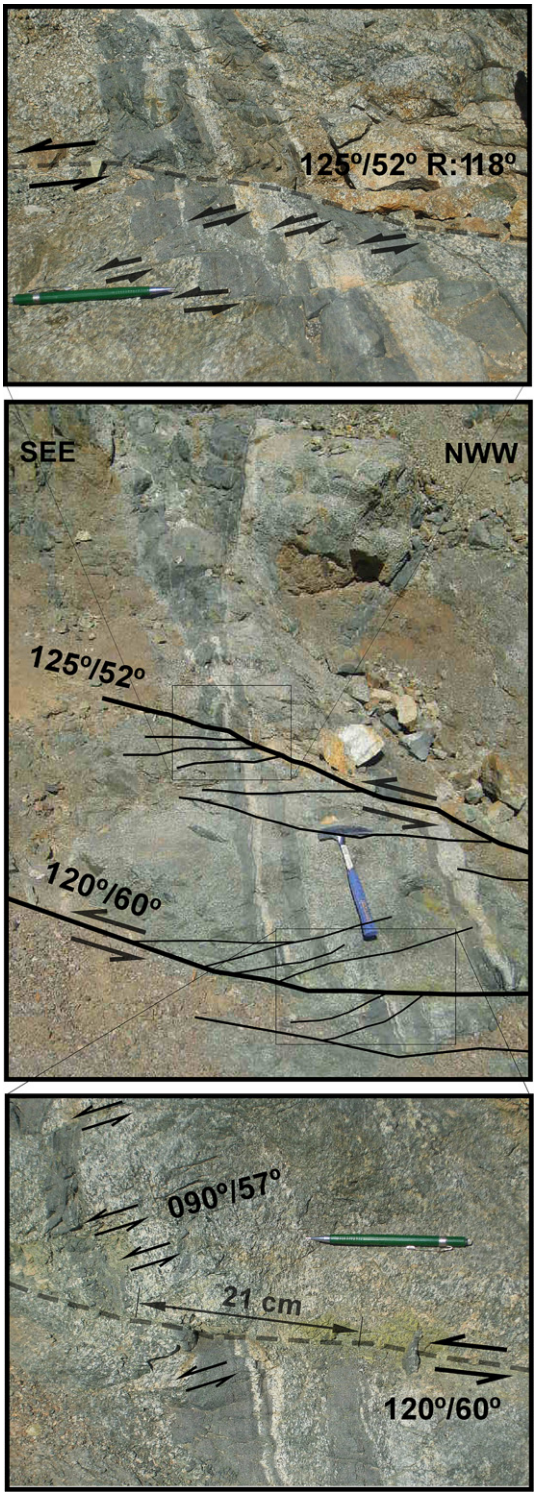

Fig. 4. Field photos within Palmera Fault. This is a representative case of a Multiple-core Fault (or Compound Faults). Note that the faults can be separated by size and orientation in two types (Main Faults, Secondary Fractures). The photography was taken obliquely to the highly irregular surface of the outcrop and (unlike Fig. 2) photos are not ortho-rectified. This can produce distortion on the scale and the real shape of the features exposed. Hammer: 40 cm-long; pencil: 15 cm-long.

different fabric (matrix/fragments ratios) that can be classified as different fault rocks. The latter, in turn, show a systematic preferred orientation between 20° and 75° counterclockwise with respect to the core boundaries and to the banded structure. These fractures cut both the cataclasites in the core and the surrounding host rock (damage zone); however, the majority is in the core like a cataclastic foliation.

4.2. Multiple strand faults

This name is given to faults consisting of several sub-parallel, centimeter–meter long and millimeter–centimeter thick faults, bearing cataclastic cores and separated by domains of systematically fractured protolith (Fig. 4). They can also be named Compound Faults as in Martel (1990). Most of the shear in the multiple strand faults is accommodated in sub-parallel faults that are separated by distances of about one order of magnitude smaller than their lengths, and here are named *Main Faults*. These Main Faults are connected by several smaller fractures with much smaller to none displacement on them, which are here named *Secondary Fractures*. It should be noted that the terms 'main' and 'secondary' are relative names used to differentiate between fractures that are distinguishable at the same scale of observation and can be applied at any scale of observation. They relate only to the relative orientation, length, and offset on these structures, and not to the timing of propagation; this issue will be addressed in the discussion.

The Main Faults show only shear displacements and the Secondary Fractures show much smaller shear displacements (down to 0) and extensional movements, with the larger opening in the center of the fractures (filled with epidote). They have a smooth sigmoidal shape, where they tend to become sub asymptotic to the Main Faults as they approach them (Fig. 5).

The geometrical and spatial distribution of these two types of fractures result in a meter-scale strike-slip duplex arrangement to the multiple strand faults.

Two examples of these Multiple-Core Faults with a duplex arrangement are Parulo and Palmera Faults, described below. Both are located around the tip point of Bolfin Fault and have left-lateral total horizontal displacement of a few meters (exceptionally some of the Main Faults show dextral displacements).

4.2.1. Parulo Fault

The Parulo Fault outcrops along the Parulo Gully (Fig. 1C) and is one of the second-order faults defining the horsetail structure of the tip point of the Bolfin Fault (Olivares, 2004). It shows a general NNW strike of 150°, has a length of about 2 km and its total thickness is ~17 m.

Fig. 2 shows an outcrop-scale structural map from part of the internal structure of Parulo Fault. In this map, the Main Faults and the Secondary Fractures can easily be identified.

The Main Faults within Parulo Fault are 3–10 m long and 3–11 mm thick. They exhibit millimetric cores of clay-rich light-green gouge layers that have sub-horizontal striae and show centimetric–metric horizontal displacements as evidenced by offsets of a mafic dike.

The Secondary Fractures, in turn, are 0.1–1 m long and 0.1–3 mm thick. Their strikes vary between 090° and 100°, with a statistical mean deflected 40° counterclockwise from the strike of the Main Faults (rose diagram in Fig. 2). These thin fractures are mostly extensional, however, small left-lateral/extension hybrid movements can be identified in the central segment of some of them. They are filled by very a thin (<1 mm) layer of chlorite and epidote, and no-striation was identified.

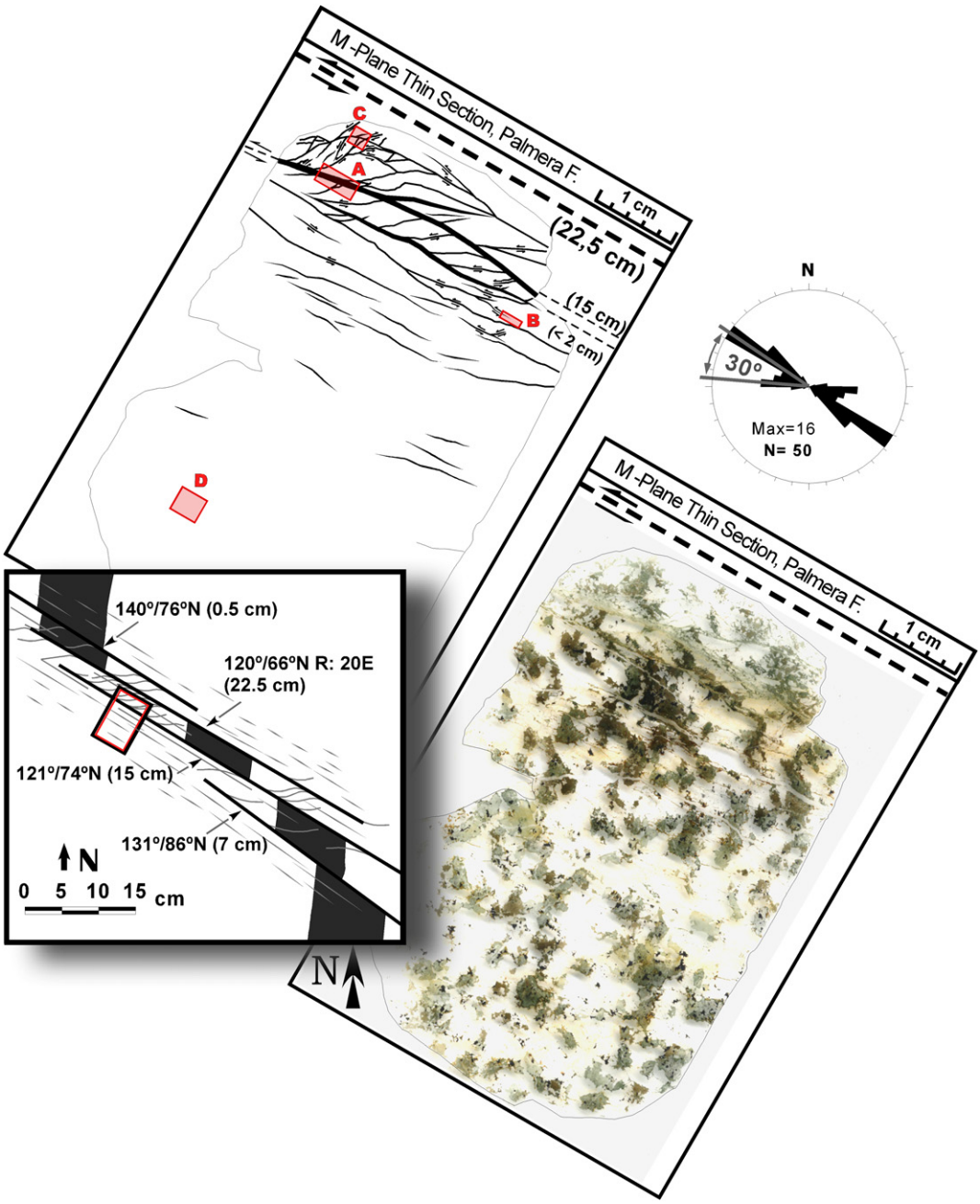

Fig. 5. Microstructural map performed over a thin section in the M-Plane of a main fault within Palmera Fault. (*i.e.* parallel to the striation and perpendicular to the fault plane). The inset is a small sketch map showing how faults are distributed and how the thin section was oriented. Horizontal left-lateral offsets of larger faults are indicated (h). Small squares with letters indicate the location of the photomicrographs in Figs. 5 and 7.

The orientation of the fractures within Parulo Fault is expressed in the equal-area diagram in the Fig. 1D, it exhibits the poles of 75 fractures (see Table 1) including main and secondary fractures measured within the fault. The mean orientation of the Secondary Faults is 097°/69° and of the Main Faults is 143°/88°S. Weighting the orientations by the sinistral horizontal displacements measured on the field (i.e. giving more importance to highest displacement faults and voiding fractures without displacement) the weighted mean direction is 148°/85°. This strike is closer to the topographic expression of the fault, given by the Parulo Gully, and this suggests that its surface expression may be controlled mostly by the larger fractures.

Both Main and Secondary Fractures exhibit felsic haloes of alteration minerals. Most of the haloes are made of albite and epidote, this gives them a characteristic white/green coloration that strongly contrasts with the oxide orange color of the weathering of the amphiboles in the meta-diorites host rock. They have variable mm to cm thickness and their scaling with the displacement is discussed in Faulkner et al. (2011).

The total horizontal displacement of the Parulo Fault was calculated by adding up the offsets of the Main Faults on transects across the fault in two different locations. The data indicate this fault exhibits an extremely low localization of the strain: Varies from 40 to 50 cm of shear displacement per meter of fault-thickness. However, it

Table 1
Fractures orientation within Palmera Fault.

Orientation (Strike°/Dip°)			H^a {m}	Structure type	Fault name	UTM position, WGS84, 19K	
						{m} East	{m} North
100	80	S	70	Main Fault	Parulo Fault	352,449	7,345,925
120	85	N	5	Main Fault	Parulo Fault	352,449	7,345,925
105	85	S	25	Main Fault	Parulo Fault	352,449	7,345,925
120	80	W	3	Main Fault	Parulo Fault	352,449	7,345,925
160	88	W	15	Main Fault	Parulo Fault	352,449	7,345,925
107	78	S	21	Main Fault	Parulo Fault	352,449	7,345,925
166	84	S	6	Main Fault	Parulo Fault	352,449	7,345,925
158	86	S	4	Main Fault	Parulo Fault	352,449	7,345,925
165	83	S	2	Main Fault	Parulo Fault	352,449	7,345,925
100	81	S	5	Main Fault	Parulo Fault	352,449	7,345,925
173	87	W	4	Main Fault	Parulo Fault	352,449	7,345,925
169	81	W	5	Main Fault	Parulo Fault	352,449	7,345,925
135	78	S	4	Main Fault	Parulo Fault	352,391	7,345,980
118	84	S	85	Main Fault	Parulo Fault	352,391	7,345,980
135	85	N	10	Main Fault	Parulo Fault	352,391	7,345,980
110	68	S	220	Main Fault	Parulo Fault	352,391	7,345,980
160	80	S	400	Main Fault	Parulo Fault	352,391	7,345,980
152	85	S	940	Main Fault	Parulo Fault	352,391	7,345,980
115	85	N	70	Main Fault	Parulo Fault	352,391	7,345,980
116	88	N	5	Main Fault	Parulo Fault	352,391	7,345,980
127	86	S	385	Main Fault	Parulo Fault	352,391	7,345,980
110	80	S	24	Main Fault	Parulo Fault	352,391	7,345,980
118	88	S	65	Main Fault	Parulo Fault	352,391	7,345,980
154	72	N	7	Main Fault	Parulo Fault	352,625	7,345,658
131	90	N	28	Main Fault	Parulo Fault	352,625	7,345,658
145	90	N	29	Main Fault	Parulo Fault	352,625	7,345,658
145	84	N	−40	Main Fault	Parulo Fault	352,625	7,345,658
134	49	N	20	Main Fault	Parulo Fault	352,625	7,345,658
137	64	N	157	Main Fault	Parulo Fault	352,625	7,345,658
141	76	N	16	Main Fault	Parulo Fault	352,625	7,345,658
110	70	S	−10	Main Fault	Parulo Fault	352,625	7,345,658
130	72	N	50	Main Fault	Parulo Fault	352,625	7,345,658
123	76	N	30	Main Fault	Parulo Fault	352,625	7,345,658
150	72	N	5	Main Fault	Parulo Fault	352,625	7,345,658
141	72	N	10	Main Fault	Parulo Fault	352,625	7,345,658
132	90	N	5	Main Fault	Parulo Fault	352,625	7,345,658
125	54	S	20	Main Fault	Parulo Fault	352,625	7,345,658
146	80	N	−5	Main Fault	Parulo Fault	352,625	7,345,658
137	78	N	30	Main Fault	Parulo Fault	352,625	7,345,658
137	78	N	10	Main Fault	Parulo Fault	352,625	7,345,658
137	78	N	10	Main Fault	Parulo Fault	352,625	7,345,658
130	75	N	120	Main Fault	Parulo Fault	352,625	7,345,658
123	72	S	40	Main Fault	Parulo Fault	352,625	7,345,658
135	80	N	14	Main Fault	Parulo Fault	352,625	7,345,658
113	75	S	10	Main Fault	Parulo Fault	352,625	7,345,658
126	70	S	40	Main Fault	Parulo Fault	352,625	7,345,658
135	75	N	15	Main Fault	Parulo Fault	352,625	7,345,658
127	80	S	30	Main Fault	Parulo Fault	352,625	7,345,658
146	72	N	30	Main Fault	Parulo Fault	352,625	7,345,658
110	66	S	0	Secondary Fracture	Parulo Fault	352,519	7,345,815
120	64	S	0	Secondary Fracture	Parulo Fault	352,519	7,345,815
108	70	S	0	Secondary Fracture	Parulo Fault	352,519	7,345,815
90	80	S	0	Secondary Fracture	Parulo Fault	352,519	7,345,815
85	78	S	0	Secondary Fracture	Parulo Fault	352,519	7,345,815
94	83	S	0	Secondary Fracture	Parulo Fault	352,519	7,345,815
100	65	S	0	Secondary Fracture	Parulo Fault	352,519	7,345,815
92	65	S	0	Secondary Fracture	Parulo Fault	352,519	7,345,815
95	63	S	0	Secondary Fracture	Parulo Fault	352,519	7,345,815
90	65	S	0	Secondary Fracture	Parulo Fault	352,519	7,345,815
80	70	S	0	Secondary Fracture	Parulo Fault	352,519	7,345,815
119	68	S	0	Secondary Fracture	Parulo Fault	352,519	7,345,815
51	86	S	0	Secondary Fracture	Parulo Fault	352,519	7,345,815
64	63	S	0	Secondary Fracture	Parulo Fault	352,519	7,345,815
90	74	S	0	Secondary Fracture	Parulo Fault	352,519	7,345,815
93	72	S	0	Secondary Fracture	Parulo Fault	352,519	7,345,815
112	30	S	0	Secondary Fracture	Parulo Fault	352,519	7,345,815
104	41	S	0	Secondary Fracture	Parulo Fault	352,519	7,345,815
108	84	N	0	Secondary Fracture	Parulo Fault	352,519	7,345,815
110	54	S	0	Secondary Fracture	Parulo Fault	352,519	7,345,815
107	89	N	0	Secondary Fracture	Parulo Fault	352,519	7,345,815
93	72	S	0	Secondary Fracture	Parulo Fault	352,519	7,345,815
115	71	S	0	Secondary Fracture	Parulo Fault	352,519	7,345,815
133	88	S	–	Mean orientation of main Faults[b]	Parulo Fault	–	–

Table 1 (*continued*)

Orientation (Strike°/Dip°)			H[a] {m}	Structure type	Fault name	UTM position, WGS84, 19K	
						{m} East	{m} North
97	68	S	–	Mean orientation of secondary fractures[c]	Parulo Fault	–	–
148	85	S	–	Weighted mean orientation[d]	Parulo Fault	–	–

[a] H is the sinistral horizontal displacement (left-lateral positive). Values smaller than 1 cm are considered to be zero (a "crack").
[b] Mean orientation of fractures with $H > 0$. Largest eigenvector of the orientation matrix (according to Woodcock, 1977).
[c] Mean orientation of fractures with $H \approx 0$. Largest eigenvector of the orientation matrix (according to Woodcock, 1977).
[d] Orientations weighted by the sinistral horizontal displacement H.

is worth noting that this is a highly heterogeneous and discrete strain distribution at outcrop scale (*i.e.*: brittle).

4.2.2. Palmera Fault

The Palmera Fault runs along the Palmera Gully, in the central area around the tip point of Bolfin Fault (see Fig. 1C) and has a general strike 120°. Its length cannot be determined in satellite or aerial imagery; however, from field observations it can be estimated to be *ca*. 1000 m long. Its minimum total thickness is 4 m, including all the decimetric to metric-long faults of which Palmera Fault is made up.

The Main Faults within this fault are mostly 1–5 m long and 1–3 mm thick. In general their trends vary between 90 and 130°, and their dips: 50°NE–50°SW. All of them exhibit shear displacement as evidenced by the offset of markers (*e.g.* subvertical dikes) or the presence of wear material (cataclastic layers) without offset markers, in which case the shear sense cannot be determined. Ridge-and-groove striae onto epidote + chlorite assemblages and dike

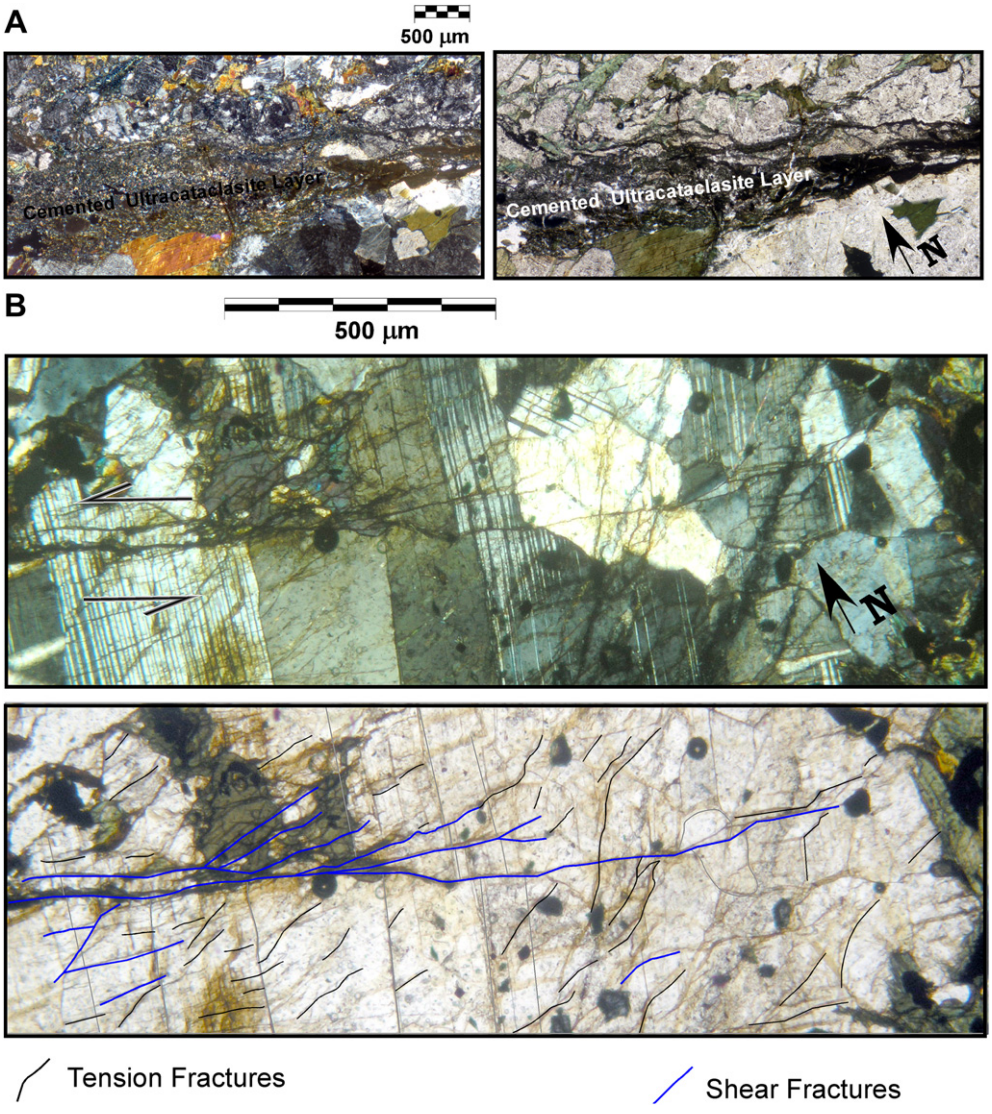

Fig. 6. Photomicrographs made in the thin section on Fig. 5. (Right: Open nicol, Left: Crossed nicol). (A) Internal structure of one of the Main Faults within Palmera Fault ($h = 15$ cm). Ultracatalasite cemented with Chlorite. (B) Horsetail structure in a small displacement Main Fault. A fracture map is included, structures colored by mode of movement. Grey lines highlight textural features that are useful as markers.

Table 2
Fractures orientation within Palmera Fault.

Orientation (Strike°/Dip°)			H[a] {m}	Structure type	Fault name	UTM position, WGS84, 19K	
						{m} East	{m} North
110	56	S	26	Main Fault	Palmera Fault	352,785	7,346,900
100	45	S	26	Main Fault	Palmera Fault	352,785	7,346,900
100	58	S	5	Main Fault	Palmera Fault	352,785	7,346,900
120	58	S	−1	Main Fault	Palmera Fault	352,785	7,346,900
93	58	S	4	Main Fault	Palmera Fault	352,785	7,346,900
110	72	S	10	Main Fault	Palmera Fault	352,785	7,346,900
120	82	S	10	Main Fault	Palmera Fault	352,785	7,346,900
111	64	S	2	Main Fault	Palmera Fault	352,785	7,346,900
100	47	S	4	Main Fault	Palmera Fault	352,785	7,346,900
93	54	N	1	Main Fault	Palmera Fault	352,785	7,346,900
52	75	S	0	Secondary Fracture	Palmera Fault	352,785	7,346,900
64	75	S	0	Secondary Fracture	Palmera Fault	352,785	7,346,900
82	75	S	0	Secondary Fracture	Palmera Fault	352,785	7,346,900
67	54	S	2	Main Fault	Palmera Fault	352,785	7,346,900
92	58	S	0	Secondary Fracture	Palmera Fault	352,785	7,346,900
82	60	S	0	Secondary Fracture	Palmera Fault	352,785	7,346,900
112	70	S	3	Main Fault	Palmera Fault	352,785	7,346,900
90	80	S	0	Secondary Fracture	Palmera Fault	352,785	7,346,900
92	82	S	0	Secondary Fracture	Palmera Fault	352,785	7,346,900
88	78	S	0	Secondary Fracture	Palmera Fault	352,785	7,346,900
90	57	S	0	Secondary Fracture	Palmera Fault	352,785	7,346,900
95	52	S	0	Secondary Fracture	Palmera Fault	352,785	7,346,900
85	60	S	0	Secondary Fracture	Palmera Fault	352,785	7,346,900
120	60	S	21	Main Fault	Palmera Fault	352,785	7,346,900
125	52	S	2	Main Fault	Palmera Fault	352,785	7,346,900
140	76	N	0	Secondary Fracture	Palmera Fault	352,752	7,346,914
120	66	N	23	Main Fault	Palmera Fault	352,752	7,346,914
121	74	N	15	Main Fault	Palmera Fault	352,752	7,346,914
131	66	N	7	Main Fault	Palmera Fault	352,752	7,346,914
76	65	N	0	Secondary Fracture	Palmera Fault	352,752	7,346,914
79	68	N	0	Secondary Fracture	Palmera Fault	352,752	7,346,914
82	71	N	0	Secondary Fracture	Palmera Fault	352,752	7,346,914
110	68	S	–	Mean orientation of Main Faults[b]	Palmera Fault	–	–
84	77	S	–	Mean orientation of Secondary Fractures[c]	Palmera Fault	–	–
112	67	S	–	Weighted mean orientation[d]	Palmera Fault	–	–

[a] H is the sinistral horizontal displacement (left-lateral positive). Values smaller than 1 cm are considered to be zero (a "crack").
[b] Mean orientation of fractures with $H > 0$. Largest eigenvector of the orientation matrix (according to Woodcock, 1977).
[c] Mean orientation of fractures with $H \approx 0$. Largest eigenvector of the orientation matrix (according to Woodcock, 1977).
[d] Orientations weighted by the sinistral horizontal displacement H.

offsets of Main Faults within Palmera Fault indicate a predominantly left-lateral strike-slip displacement, with a vertical component less than 40% of the horizontal movement.

Secondary Fractures, in turn, are 5–500 mm long and between 10 and 100 μm thick. These small fractures show smooth sigmoidal shapes with an average trend deflected 30° counterclockwise from the average trend of the Main Faults. Microscopic analysis shows that some of these fractures are tensional, but most of them are small shear fractures or "microfaults" with hybrid movement (see Figs. 5 and 6). Millimetric displacements in these microfaults produce thin cataclasite layers or displaced crystal boundaries.

The orientation of the fractures within Parulo Fault is expressed in the equal-area diagram in the Fig. 1E, it exhibits the poles of 35 fractures (see Table 2) including main and secondary fractures measured within the fault. The mean orientation of the Secondary Faults is 084°/77° and of the Main Faults is 110°/68°S. The horizontal displacement weighted mean direction is 112°/67°.

Fig. 5 shows a microstructural map made from a thin section of the M-plane or "plane of movement" (*i.e.* the plane parallel to striation and perpendicular to the fault plane) of a metric fault, oriented 120°/66°NE and a striation with rake 020° NW (a Main Fault).

Main and Secondary Fractures are easily identified in this thin section; they form a milimetric-scale strike-slip duplex structure (similar to hosting, kilometric-scale Caleta Coloso Duplex), and decrease in density away from the largest fault.

Although all of the microfractures in the map of Fig. 5 exhibit an evident decrease in density away from the largest displacement fault (22.5 cm), Main Faults dominate over Secondary Fractures. The former are heterogeneously distributed over an area of a 47 cm around the largest displacement fault. The latter, in turn, are located in a narrower zone (20 cm), only in areas between Main Faults and more concentrated between faults with larger displacements (>5 cm).

As can be observed in the photomicrograph (Figs. 6 and 7) most of the microfaults and fractures are sealed or cemented by the precipitation of neo-formed minerals (epidote, chlorite or phyllosilicates). In their cores, some of the microfaults host fragments of plagioclase from the protolith or restrained neo-formed minerals (Fig. 6A).

Associated with the microfaults, other straight and narrow shear discontinuities can also be identified producing offsets of the plagioclase twins. These are straight microscopic shear bands, 10–400 microns long and left-lateral offsets (synthetic to the main sense of shear). The facts that no crystallographic discontinuity was recognized across them and that twins terminate at this deformation bands and do not follow within them, suggest that these bands represent healed shear fractures (as in Stünitz et al., 2003) (Fig. 7C).

In close spatial and geometrical relationships with the microfaults also can be recognized some evidences of plastic deformation:. Deformation twins, undulatory extinction and bending of

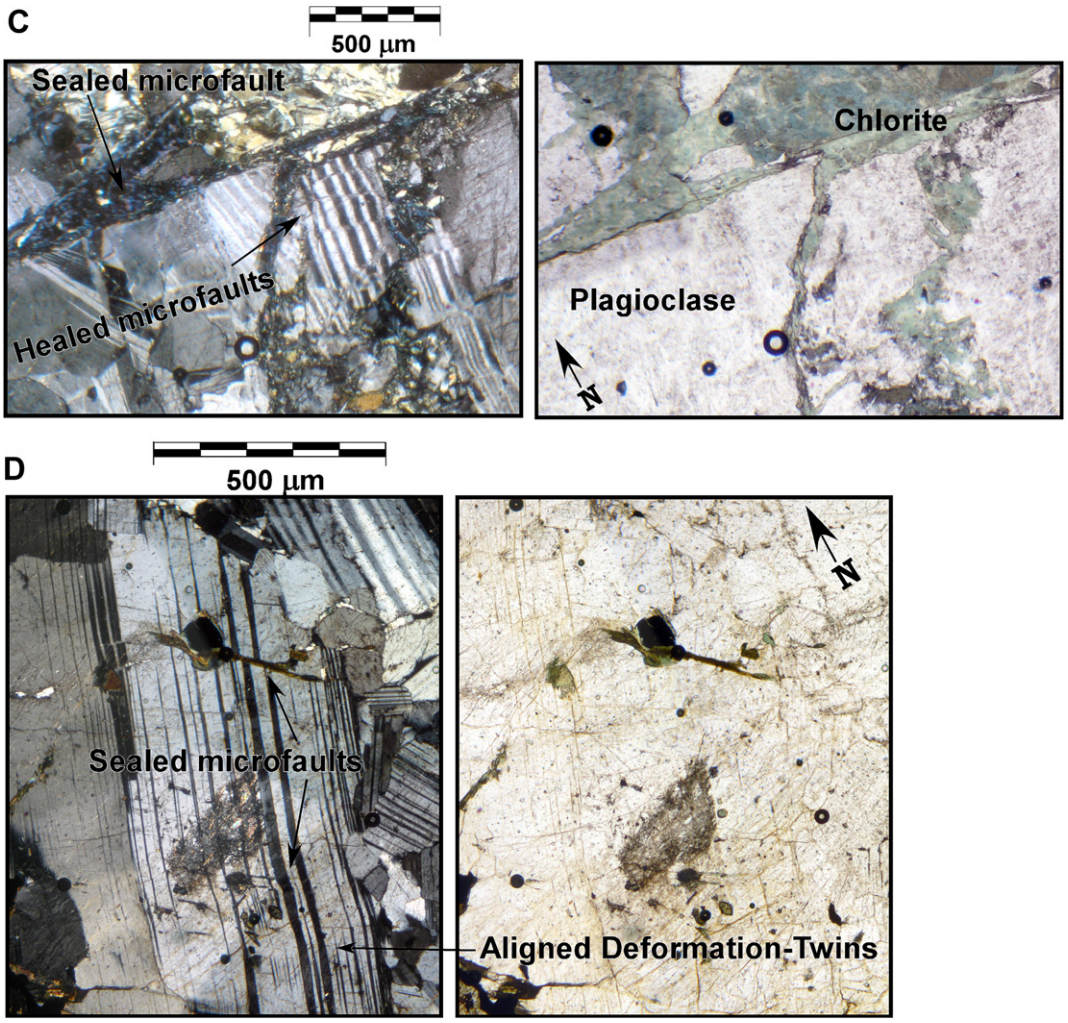

Fig. 7. Photomicrographs made in the thin section on Fig. 5. (Right: Open nicol, Left: Crossed nicol). (C) Sealed-fractures, sealed with hydrothermal chlorite, and healed shear fracture, evidenced by small plagioclase left-lateral dislocations. (D) Plagioclase crystal with left-lateral shear-strain. The configuration of the deformational twins and the sealed fractures, suggest that it suffered both plastic and brittle deformation.

crystal boundaries can be observed in the plagioclase crystals of the protolith under the petrographic light microscope (Fig. 7D).

5. Discussion

5.1. Multiple scale strike-slip duplex geometry

According to the data presented here, the strike-slip duplex pattern is the most characteristic feature in the geometry of the fault arrangements at all scales. This pattern can be observed at the regional scale, in the Atacama Fault System (Caleta Coloso Duplex in Cembrano et al., 2005); at outcrop- or metric-scale, in the Parulo and Palmera Fault internal structure; and at millimetric-scale, in the thin section of Palmera Fault (Fig. 8).

The presence of this duplex pattern in fault arrangements has been also previously observed in other metric to kilometric-scale fault systems. *e.g.*: three Pagodas and Mae ping fault zones, western Thailand (Morley, 2004; Morley et al., 2007); in the Sierra Nevada, California (Flodin and Aydin, 2004; Kirkpatrick et al., 2008; Martel, 1990; Martel et al., 1988); and in the Italian Southern Alps (Di Toro and Pennacchioni, 2005). However, none of these works include observations from such a wide scale range, and none describes a strike-slip duplex pattern in the internal structure of a fault that is part of larger duplex. In turn, the duplex fault systems described here are self-similar, as the same structure appears repeated on a range of scales (Mandelbrot, 1967). Specifically, the geometry of the Caleta Coloso Duplex is repeated in the geometry of fractures in the Secondary Fractures of the Duplex (Parulo and Palmera Faults). This self-similarity suggests that the same processes control the fault propagation at all scales and, subsequently, are scale-invariant processes.

In mathematics, the term "self-similar" refers to a system that is exactly or approximately similar to a part of itself. Applied to geometrical patterns, self-similar is a shape that is systematically similar to one or more parts of it (Mandelbrot, 1967). That is exactly the case of the geometry presented by the structures forming the Caleta Coloso Duplex, over seven orders of magnitude. The duplex pattern is self-similar as can clearly be seen in the log–log plot of the Fig. 9.

The length (L) and width (W) of 22 duplexes and faults forming them, at several scales, are plotted in the log–log diagram of Fig. 9. The smaller scale data, coming from Palmera and Parulo Fault sites, were obtained from the internal structure of the faults as described in a previous section. The larger scale data were taken from a previously published work in the same area (Cembrano et al., 2005). Data in Fig. 9 are best fit by a power law relationship:

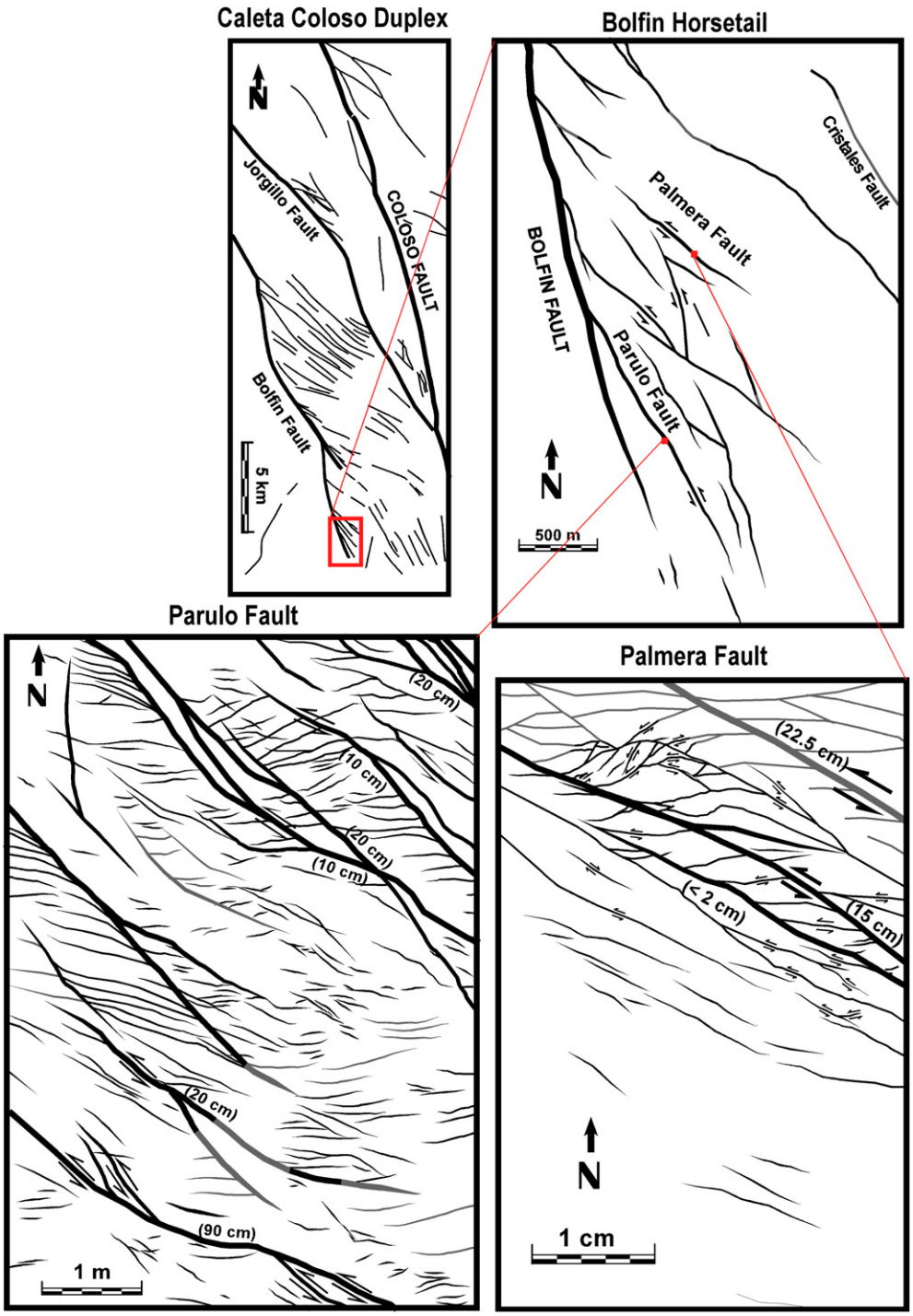

Fig. 8. Summary sketch showing the geometry of the described structural system at all the described scales. The structural maps are extracts from the maps shown in Figs. 1, 2 and 5, slightly modified. Grey lines were added to fill the covered and not mapped areas based in the surrounding structures, and in the horsetail map some lines where smoothed in order to decrease the strong effect of the topography on the shape of the fault traces. Thicker lines are the largest fault with larger horizontal displacements (marked between parentheses).

$$L = 10^{1.1} \cdot W^{0.9}$$

where W is the width of the duplex and L is the average length between the two Main Faults forming each duplex as represented in the sketch of Fig. 9.

The results are internally consistent and essentially show an almost linear relationship between the mean length of the main duplex faults and the duplex width. In other words, for a scale range of seven orders of magnitude, the length of the master strike-slip faults is about 10 times the width of the overlapping duplex area. This relationship, apart from reinforcing the self-similar nature of the structural system under study, suggests that the same fundamental mechanical processes that build up the small strike-slip duplexes operate also at the regional scale.

The distance between the Main Faults of a given duplex (or of a multiple-duplex fracture pattern) has an important meaning in the propagation of a fault trough the linking of sub-parallel smaller

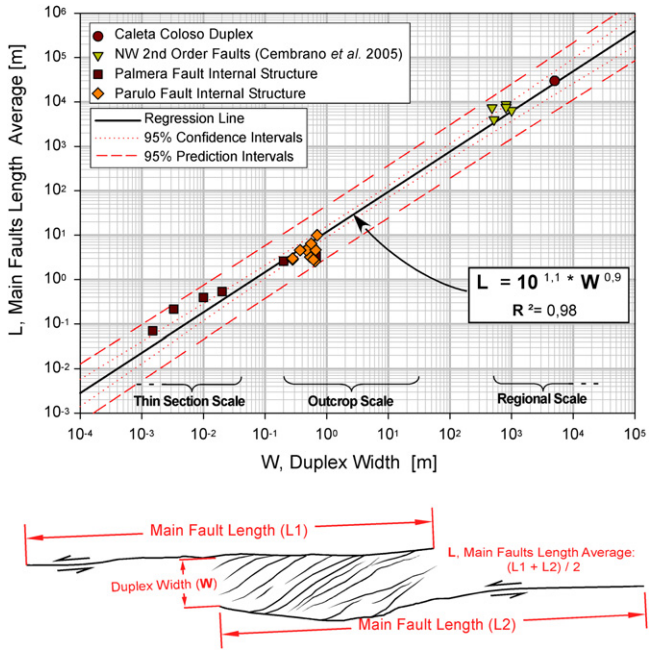

Fig. 9. Log–log plot showing the self-similarity of the duplex pattern in the described structures. The distance between Main Faults represents the duplex size or width, and it scales almost linearly with the length of the faults forming the duplexes. A linear relation would be ($A = K * L$). The overlapping "Main Faults" within the systems form duplexes almost one order of magnitude smaller than their lengths.

faults. Each primordial Main Fault can be considered to have its own stress field perturbation around and the propagation of splay and linking faults are expected to be controlled by the size and shape of such stress field, and the interaction between them.

The distance between Main Faults scales with the length of them (Fig. 9) and the stress perturbations are also a function of the fault length (and displacement) (see Homberg et al., 1997). This strongly suggests that the interaction between the stress field perturbations around primordial Main Faults controlled the size of the duplexes in the fault system at all scales. Otsuki and Dilov (2005) based on experimental work of fault zone progressive development, demonstrated that fault zones grow keeping a self-similar hierarchical structure, similar to that found on this and other previous field studies of strike-slip faults at various scales (*e.g.* Joussineau and Aydin, 2009 and references therein). Furthermore Otsuki and Dilov (2005) successfully derived the Gutenberg–Richter's law as well as the previously documented relationship of seismic nucleation sizes to seismic moments, suggesting that any seismic rupture nucleates at a smaller jog of a lower hierarchical rank and eventually terminates at a larger jog of a higher rank, which in turn is consistent with the hierarchical fault zone geometry we see in both nature and experiments.

Self-similarity has been also previously documented in structures related to plastic deformation of rocks. S-C fabrics in mylonites show a self-similar relationship in the distance between S planes against the distance between C planes (Hippertt, 1999).

5.2. Timing and mechanism of fault development

One of the most important topics in the understanding of the development of fault systems in the brittle crust is to deduce the relative timing of recognized structures.

Here, all the faults in the self-similar system (Parulo, Palmera, Bolfín and Jorgillo) are cemented with the same mineral assemblage (epidote–chlorite) and show synthetic displacements, then can be considered to be contemporaneous at geological time scale. However, they were not propagated instantly at the same moment in time, so they have different relative time occurrences at short-term scales. Furthermore, previous researchers (Herrera et al., 2005) have postulated that the fault related mineralization occurred by seismic pumping depressurization mechanism (Sibson, 1987; Sibson et al., 1975), that is an evidence of propagation by discrete events through the time.

A reliable relative timing between the Main Faults and Secondary Fractures can be deduced from the microstructural map made in the thin section on Palmera Fault (Fig. 5). If we consider that the damage area around a fault increases with the increasing total fault displacement (Chester et al., 2004; Mitchell and Faulkner, 2009; Scholz, 1987; Scholz and Aviles, 1986) and that the most proximal areas to the Main Faults show more accumulated deformation than the distal ones; then we must consider the proximal areas represent the more mature in terms of accumulated deformation. Accordingly, the deformation occurring away from the largest fault will represent the initial stages of deformation and the evolution can be deduced observing structures at intermediate distances. As seen in the thin section (Fig. 5), both Main Faults and Secondary Fractures decrease away from the largest displacement fault. However, the Secondary Fractures become relatively less common with distance from the high displacement domain. This is evidence that the Main Faults were the first structures to form in the sequence and then the Secondary Fractures started to propagate between them as linking structures. Then, they progressively kept accommodating the bulk displacement together.

Notwithstanding, although the relative timing of the fractures is understood, the mechanism by which the described faults nucleated and propagated through the crystalline rock is still not fully clear. However, a general idea can be obtained from microscopic observations. On Fig. 6B a microscopic horsetail structure at the tip point of a milimetric-displacement microfault is shown. This horsetail structure consists of very small faults producing micrometric offsets and some of them have extension cracks in their termination. This configuration suggests that the Secondary Fractures were nucleated from the earlier parallel Main Faults to the area between them or away from them. The fact that the Secondary Fractures within the Parulo Fault are mostly extensional and have almost the same orientation than Secondary Fractures within Palmera Fault suggest that Secondary Fractures have been initially propagated as tensional or "wing" cracks and were sheared later.

The propagation of the Main Faults, in turn, is the most difficult topic to elucidate from the field data. Previous works in fractures system with very similar geometry have proposed that the Main Faults (or "Master Faults") actually were joints that later become sheared during fault development (Di Toro and Pennacchioni, 2005; Flodin and Aydin, 2004; Kirkpatrick et al., 2008; Martel, 1990; Martel et al., 1988). However, the data provided here by the thin section made in Palmera Fault (Fig. 5) suggest that fractures did not initiate from significant pre-existing joints. In the section, a negative gradient of fracture density and microfault length can be observed with distance from the larger faults. Hence shear fractures become less abundant and smaller in length with distance from the larger structures. This fact, in addition with the fact that the studied outcrops do not display any systematic joint system, indicates that the Main Faults propagated as faults and not as joints.

The propagation of faults through crystalline rocks (*i.e.* Mode II and III fractures) has been strongly studied by laboratory experiments (Cox and Scholz, 1988; Petit and Barquins, 1988; Wibberley et al., 2000) and field measurements (Cowie and Scholz, 1992). The resulting conceptual models agree that faults propagate by nucleation and interaction of tensile fracture arrays ahead of the fault

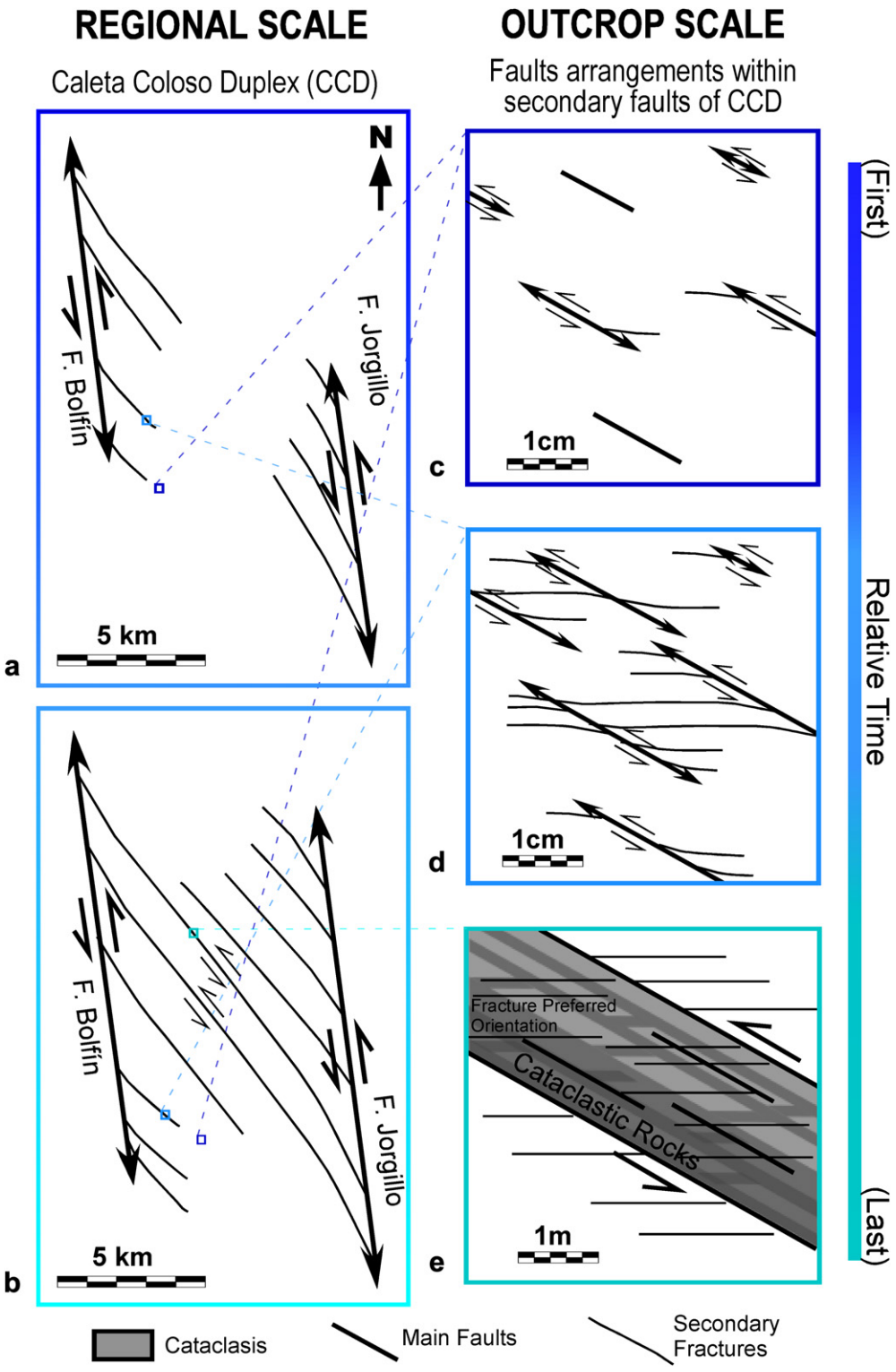

Fig. 10. Schematic sketch of the model of development of the whole analyzed fault system. At kilometric-scale (a, b) and at centimetric to metric-scale (c, d, e).

termination. These tensile fractures or cracks, should distribute randomly around all the rock, but concentrate in areas around the fault plane (as a "damage zone") and around the edges of the faults or tip lines (as a "process zone").

The faults observed here under the light microscope show not such important concentrations of cracks, neither in the fault terminations nor around the fault plane. This fact, contrasts with the intense cracking required in the mentioned conceptual models, however, it can be explained in two ways:

(1) The above-mentioned propagation models are based and focused on faulting under pure brittle conditions, through a perfectly elastic material. Instead, the faults described here exhibit mechanical twinning and undulatory extinction

coalescing with brittle dilatants fractures (Fig. 7D) that is an evidence of simultaneous brittle and plastic deformation of the plagioclase (Stünitz et al., 2003). This plasticity involves a ductile deformation of the rock, especially around terminations of shear fractures (Stünitz et al., 2003). Then, the ductile bending and shearing accommodating deformation around tip points, in the process zone, will reduce the required cracking. The fault propagation accompanied by permanent ductile deformation must then not be explained by the same models used for complete brittle–elastic conditions.

(2) The observed healed fractures and the intense mineralization activity evidenced by the sealed fractures (Figs. 6 and 7) suggest that the fault system was propagated under hydrothermal conditions (Herrera et al., 2005). These hydrothermal fluids have enhanced the diffusion process favoring healing of fractures. This strong healing may have deleted the possible previous existing cracks.

We propose that the studied Main Faults were propagated by the generation and coalescing of cracks, but inhibited by the ongoing coeval plastic processes. Furthermore, the coeval hydrothermal activity probably continuously annihilated the cracks around faults by fracture healing (Stünitz et al., 2003).

5.3. Multi-scale model of development

The proposed model of development of the multiple-duplex fault system is shown on Fig. 10 for three scales of observation. In this model, we postulate that the regional-scale faults start as families of relatively smaller fractures (extensional and shear) that progressively and heterogeneously concentrate until becoming multiple-duplex fault zones and then become mature fault zones. That evolution trough a progressive concentration of fractures, or fault "maturation", is in complete agreement with previous laboratory observations (Lockner et al., 1991). Furthermore, we propose here that this occurs by the progressive propagation of fractures oriented between 15° and 75° (measured in the sense of slip) from Main Faults. Lately, in the mature fault zones, this fracturing keeps occurring heterogeneously generating cataclastic rocks in the most damaged regions, resulting on a banded cataclastic core with fracture preferred orientation.

Although the evidence to deduce such fault evolution have been mainly observed at microscopic- and metric-scale, it can also be inferred to occur at larger scales, as the system is self-similar.

Then, the banded cataclastic core observed in the internal structure of large-scale faults in the AFS (*e.g.*: Bolfin Fault: Jensen, 2008, and Fig. 1; Coloso Fault: Mitchell, 2007; Mitchell and Faulkner, 2009; and Faulkner et al., 2008) would be the result of the progressive fracturing described above, interacting and mechanically aided by hydrothermal fluids.

6. Conclusions

- The strike-slip duplex pattern is the most characteristic feature in the geometry of the studied fault arrangements at all scales. The presence of this pattern at all scales form a self-similar strike-slip duplex system.
- The mesoscopic faults in the Duplex Caleta Coloso can be separated according to the internal structure into two types: *Single-Core Faults* and *Multiple Strands Faults* (or Compound Faults)
- The progressive fracturing oriented between 15° and 75° counterclockwise from the main shear plane (measured in the slip sense) has been the main deformation process building the geometry of the described strike-slip duplex system in the Atacama Fault System. During initial stages, this fracturing linked subparallel faults in slow-strain fault zones (Multiple-Core Faults). Later, with increasing strain, these slow-strain faults evolved to become cataclastic zones where the fracturing continued to occur, producing fracture preferred orientations.
- The propagation of the fault system occurred under upper-crustal hydrothermal conditions enhancing some crystal-scale processes of fracture sealing and healing and brittle-plastic conditions evidenced by deformation twinning and undulatory extinction around microfaults.
- Mean length to width ratios for the studied strike-slip duplexes at a wide range of scales is fairly constant showing a remarkably well-constrained self-similarity of the structural system, which in turn appears to be consistent with how earthquake ruptures nucleate and propagate in both experiments and nature.

Acknowledgments

Thanks to all the colleagues at the Departamento de Ciencias Geológicas UCN who help to develop this work. To Pamela Perez, Rodrigo Gomila, Felipe Aron, Pía Ávalos, Tito Álvarez and Rodrigo Carle, for hard working in the field and having essential brainstorm discussions. Special thanks to Professors Gabriel Gonzalez, Eduardo Medina and Hans Wilke.

Thanks also to the professor Mark Handy, that kindly help on the recognition of microstructures from photomicrographs.

Tom Mitchell is thanked for comments and discussion that helped us to improve the manuscript.

FONDECYT PROJECTS 1020436 and 1100464 granted to JC and GA have funded most of the field work presented here. A master thesis research grant to EJ by Universidad Católica del Norte helped to fund the laboratory work. CONICYT project AT 24091112 also funded the development of this paper. We would also like to thank the editor Joao Hippert and the reviewers Fabrizio Storti and Fernando Hongn for their helpful comments that greatly improved the science of this manuscript.

References

Arabasz, W.J., 1971. Geological and Geophysical Studies of the Atacama Fault Zone in Northern Chile. Ph.D. thesis, California Institute of Technology, Passadena, 275 pp.

Barton, C.A., Zoback, M.D., Moos, D., 1995. Fluid flow along potentially active faults in crystalline rock. Geology 23 (8), 683–686.

Brown, M., Diaz, F., Grocott, J., 1993. Displacement History of the Atacama Fault System 25°00′S–27°00′S, Northern Chile. Geological Society of America Bulletin 105 (9), 1165–1174.

Cembrano, J., González, G., Arancibia, G., Ahumada, I., Olivares, V., Herrera, V., 2005. Fault zone development and strain partitioning in an extensional strike-slip duplex: a case study from the Mesozoic Atacama fault system, Northern Chile. Tectonophysics 400 (1–4), 105–125.

Connolly, P., Cosgrove, J., 1999. Prediction of static and dynamic fluid pathways within and around dilational jogs. In: Geological Society of London, Special Publications, vol. 155 (1), pp. 105–121.

Cowie, P.A., Scholz, C.H., 1992. Physical explanation for the displacement length relationship of faults using a post-yield fracture-mechanics model. Journal of Structural Geology 14 (10), 1133–1148.

Cox, S.J.D., Scholz, C.H., 1988. On the formation and growth of faults: an experimental study. Journal of Structural Geology 10 (4), 413–430.

Cox, S.F., 1999. Deformational controls on the dynamics of fluid flow in mesothermal gold systems. In: Geological Society of London, Special Publications, vol. 155 (1), 123–140.

Chester, F.M., Chester, J.S., Kirschner, D.L., Schulz, S.E., Evans, J.P., 2004. Structure of large-displacement, strike-slip fault zones. In: Karner, G.D., Taylor, B., Driscoll, N.W., Kohlstedt, D.L. (Eds.), Rheology and Deformation.

Di Toro, G., Pennacchioni, G., 2005. Fault plane processes and mesoscopic structure of a strong-type seismogenic fault in tonalites (Adamello batholith, Southern Alps). Tectonophysics 402 (1–4), 55–80.

Faulkner, D.R., Mitchell, T.M., Healy, D., Heap, M.J., 2006. Slip on 'weak' faults by the rotation of regional stress in the fracture damage zone. Nature 444 (7121), 922–925.
Faulkner, D.R., Mitchell, T.M., Rutter, E.H., Cembrano, J., 2008. On the structure and mechanical properties of large strike-slip faults. In: Geological Society, London, Special Publications, 299 (1), pp. 139–150.
Faulkner, D.R., Mitchell, T.M., Jensen, E., Cembrano, J, 2011. The scaling of fault damage zones with displacement and the implications for fault growth processes. Journal of Geophysical Research 116, B05403. doi:10.1029/2010JB007788.
Flodin, E.A., Aydin, A., 2004. Evolution of a strike-slip fault network, Valley of Fire State Park, southern Nevada. Geological Society of America Bulletin 116 (1–2), 42–59.
Fuenzalida, V., 1965. Clima. In: Geografía Económica de Chile. CORFO, Santiago, pp. 95–152.
Gibson, R.G., 1994. Fault-zone seals in siliciclastic strata of the Columbus Basin, offshore Trinidad. AAPG Bulletin 78 (9), 1372–1385.
González, G., 1996. Evolución tectónica de la Cordillera de la Costa de Antofagasta (Chile): Con especial referencia a las deformaciones sinmagmáticas del Jurásico-Cretácico Inferior. PhD thesis, Freïe Universität Berlin.
Gonzalez, G., Carrizo, D., 2003. Segmentation, kinematics and relative chronology of the late deformation of Salar del Carmen Fault, Atacama Fault System (23 degrees 40′S), northern Chile. Revista Geologica De Chile 30 (2), 223–244.
Grocott, J., Taylor, G.K., 2002. Magmatic arc fault systems, deformation partitioning and emplacement of granitic complexes in the Coastal Cordillera, north Chilean Andes (25°30′S to 27°00′S). Journal of the Geological Society 159 (4), 425–443.
Herrera, V., Cembrano, J., Olivares, V., Kojima, S., Arancibia, G., 2005. Precipitation by depressurization and boiling in veins hosted in an extensional strike-slip duplex: microstructural and microthermometric evidence. Revista Geologica De Chile 32 (2), 207–227.
Hippertt, J., 1999. Are S-C structures, duplexes and conjugate shear zones different manifestations of the same scale-invariant phenomenonen? Journal of Structural Geology 21 (8), 975–984.
Homberg, C., Hu, J., Angelier, J., Bergerat, F., Lacombe, O., 1997. Characterization of stress perturbations near major fault zones: Insights from 2-D distinct-element modelling and field studies (Jura Mountains). Journal of Structural Geology 19 (5), 703–718.
Jensen, E., 2008. Deformación progresiva de fallas de rumbo, el caso de la Falla Bolfín. Memoria para optar al título de geólogo. MSc thesis. Universidad Católica del Norte, Antofagasta, Chile.
Joussineau, G., Aydin, A., 2009. Segmentation along strike-slip faults revisited. Pure and Applied Geophysics 166 (19).
Kirkpatrick, J.D., Shipton, Z.K., Evans, J.P., Micklethwaite, S., Lim, S.J., McKillop, P., 2008. Strike-slip fault terminations at seismogenic depths: The structure and kinematics of the Glacier Lakes fault, Sierra Nevada United States. Journal of Geophysical Research 113 (B4), B04304.
Lange, D., Cembrano, J., Rietbrock, A., Haberland, C., Dahm, T., Bataille, K., 2008. First seismic record for intra-arc strike-slip tectonics along the Liquiñe-Ofqui fault zone at the obliquely convergent plate margin of the southern Andes. Tectonophysics 455 (1–4), 14–24.
Lockner, D.A., Byerlee, J.D., Kuksenko, V., Ponomarev, A., Sidorin, A., 1991. Quasi-static fault growth and shear fracture energy in granite. Nature 350 (6313), 39–42.
Mandelbrot, B., 1967. How long is the coast of Britain? Statistical self-similarity and fractional dimension. Science 156 (3775), 636–638.
Martel, S.J., 1990. Formation of compound strike-slip fault zones, Mount Abbot quadrangle, California. Journal of Structural Geology 12 (7), 869–877. 879–882.
Martel, S.J., Pollard, D.D., Segall, P., 1988. Development of simple strike-slip-fault zones, Mount Abbot Quadrangle, Sierra-Nevada, California. Geological Society of America Bulletin 100 (9), 1451–1465.
Mitchell, T.M., 2007. The Fluid Flow Properties of Fault Damage Zones. PhD thesis, Harold Cohen Library, University of Liverpool.
Mitchell, T.M., Faulkner, D.R., 2009. The nature and origin of off-fault damage surrounding strike-slip fault zones with a wide range of displacements: a field study from the Atacama fault system, northern Chile. Journal of Structural Geology 31 (8), 802–816.
Moir, H., Lunn, R.J., Shipton, Z.K., Kirkpatrick, J.D., 2010. Simulating brittle fault evolution from networks of pre-existing joints within crystalline rock. Journal of Structural Geology 32 (11), 1742–1752.
Morley, C.K., 2004. Nested strike-slip duplexes, and other evidence for Late Cretaceous-Palaeogene transpressional tectonics before and during India-Eurasia collision, in Thailand, Myanmar and Malaysia. Journal of the Geological Society 161 (5), 799–812.
Morley, C.K., Smith, M., Carter, A., Charusiri, P., Chantraprasert, S., 2007. Evolution of deformation styles at a major restraining bend, constraints from cooling histories, Mae Ping fault zone, western Thailand. In: Geological Society of London, Special Publications, vol. 290 (1), 325–349 pp.
Olivares, V., 2004. Geometría y cinemática del sistema de fallas y vetas de la porción sur del Duplex Caleta Coloso, región de Antofagasta., Universidad Católica del Norte.
Otsuki, K., Dilov, T., 2005. Evolution of hierarchical self-similar geometry of experimental fault zones: implications for seismic nucleation and earthquake size. Journal of Geophysical Research 110, B03303.
Petit, J.-P., Barquins, M., 1988. Can natural faults propagate under mode II conditions? Tectonics 7 (6), 1243–1256.
Sanderson, D.J., Zhang, X., 2004. Stress-controlled localization of deformation and fluid flow in fractured rocks. In: Geological Society of London, Special Publications, vol. 231 (1) 299–314 pp.
Scheuber, E., Andriessen, P.A.M., 1990. The Kinematic and Geodynamic Significance of the Atacama Fault Zone, Northern Chile. Journal of Structural Geology 12 (2), 243–257.
Scheuber, E., González, G., 1999. Tectonics of the Jurassic–Early Cretaceous magmatic arc of the north Chilean Coastal Cordillera (22 degrees–26 degrees S): A story of crustal deformation along a convergent plate boundary. Tectonics 18 (5), 895–910.
Scheuber, E., Hammerschmidt, K., Friedrichsen, H., 1995. Ar-40/Ar-39 and Rb–Sr analyses from ductile shear zones from the Atacama Fault Zone, Northern Chile – the age of deformation. Tectonophysics 250 (1–3), 61–87.
Scheuber, E., Reutter, K.J., 1992. Magmatic arc tectonics in the Central Andes between 21°S and 25°S. Tectonophysics 205 (1-3), 127–140.
Scholz, C.H., 1987. Wear and gouge formation in brittle faulting. Geology 15 (6), 493–495.
Scholz, C.H., Aviles, C.A., 1986. The fractal geometry of faults and faulting. In: Das, S., Boatwright, J., Scholz, C. (Eds.), Earthquake Source Mechanics. Academic Press, New York, p. 9.
Scholz, C., Dawers, N., Yu, J.Z., Anders, M., Cowie, P., 1993. Fault growth and fault scaling laws: preliminary results. Journal of Geophysical Research 98 (B12), 21951–21961.
Sibson, R.H., 1977. Fault rocks and fault mechanisms. Journal of the Geological Society 133 (3), 191–213.
Sibson, R.H., 1994. Crustal stress, faulting and fluid flow. In: Geological Society of London, Special Publications, vol. 78 (1) 69–84.
Sibson, R.H., 1985. Stopping of earthquake ruptures at dilational fault jogs. Nature 316 (6025), 248–251.
Sibson, R.H., 1987. Earthquake rupturing as a mineralizing agent in hydrothermal systems. Geology 15 (8), 701–704.
Sibson, R.H., Moore, J.M.M., Rankin, A.H., 1975. Seismic pumping – a hydrothermal fluid transport mechanism. Journal of the Geological Society 131 (6), 653–659.
Sillitoe, R.H., 1973. The tops and bottoms of porphyry copper deposits. Economic Geology 68 (6), 799–815.
Smith, D.A., 1980. Sealing and nonsealing faults in Louisiana Gulf Coast salt basin. American Association of Petroleum Geologists Bulletin (United States) 64, 145–172.
Stünitz, H., Fitz Gerald, J.D., Tullis, J., 2003. Dislocation generation, slip systems, and dynamic recrystallization in experimentally deformed plagioclase single crystals. Tectonophysics 372 (3-4), 215–233.
Swanson, M.T., 2006. Late Paleozoic strike-slip faults and related vein arrays of Cape Elizabeth, Maine. Journal of Structural Geology 28 (3), 456–473.
Sylvester, A.G., 1988. Strike-slip faults. Geological Society of America Bulletin 100 (11), 1666–1703.
Tomlinson, Blanco, 1997a. Structural evolution and displacement history of West Fissure fault system. Precordillera, Chile. Part 1, Synmineral Hystory. In: 8° Congreso Geológico Chileno, Antofagasta, pp. 1873–17877.
Tomlinson, Blanco, 1997b. Structural evolution and displacement history of West Fissure fault system. Precordillera, Chile. Part 1, Postmineral Hystory In: 8° Congreso Geológico Chileno, Antofagasta, pp. 1873–17877.
Wibberley, C.A.J., Petit, J.P., Rives, T., 2000. Micromechanics of shear rupture and the control of normal stress. Journal of Structural Geology 22 (4), 411–427.
Wibberley, C.A.J., Yielding, G., Di Toro, G., 2008. Recent advances in the understanding of fault zone internal structure: a review. In: Geological Society of London, Special Publications, vol. 299 (1), pp. 5–33.
Woodcock, N.H., 1977. Specification of fabric shapes using an eigenvalue method. Bulletin of Geological Society of America 88, 1231–1236.